Experimental and theoretical spectroscopic study and structural determination of nickel(II) tridentate Schiff base complexes

ARTICLE *in* SPECTROCHIMICA ACTA PART A MOLECULAR AND BIOMOLECULAR SPECTROSCOPY · MAY 2015

Impact Factor: 2.35 · DOI: 10.1016/j.saa.2015.05.084 · Source: PubMed

4 AUTHORS, INCLUDING:

ali hossein Kianfar
Isfahan University of Technology
33 PUBLICATIONS **406** CITATIONS
SEE PROFILE

Parin Dehghani
Isfahan University of Technology
2 PUBLICATIONS **2** CITATIONS
SEE PROFILE

Hamid Reza Khavasi
Shahid Beheshti University
345 PUBLICATIONS **3,033** CITATIONS
SEE PROFILE

Spectrochimica Acta Part A: Molecular and Biomolecular Spectroscopy 150 (2015) 220–229

Contents lists available at ScienceDirect

Spectrochimica Acta Part A: Molecular and Biomolecular Spectroscopy

journal homepage: www.elsevier.com/locate/saa

Experimental and theoretical spectroscopic study and structural determination of nickel(II) tridentate Schiff base complexes

Ali Hossein Kianfar [a,*], Hossein Farrokhpour [a], Parin Dehghani [a], Hamid Reza Khavasi [b]

[a] Department of Chemistry, Isfahan University of Technology, Isfahan 84156-83111, Iran
[b] Department of Chemistry, Shahid Beheshti University, G. C., Evin, Tehran 1983963113, Iran

HIGHLIGHTS

- Novel nickel Schiff base complexes were prepared and their structures were confirmed by different techniques.
- The X-ray crystallography results show that they are four coordinated in the solid state.
- DFT calculation of the UV–Visible of the complexes.

GRAPHICAL ABSTRACT

Some new tridentate Schiff base complexes of [NiL(PR_3)] (where L = (E)-1- [(2-amino-5-nitrophenyl)iminio-methyl]naphthalene-2-olate (L^1), (E)-1-[(2-hydroxiphenyl)iminio-methyl]naphthalene-2-olate (L^2), R = Bu and Ph) were synthesized and characterized by IR, UV–Vis, ^{1}H-NMR spectroscopy and elemental analysis. The geometry of [NiL^1(PBu_3)] and [NiL^2(PBu_3)] were determined by X-ray crystallography. The theoretical calculations were also performed to optimize the structure of ligands and complexes in the liquid and gas phase. The UV–Visible and IR spectra of complexes were calculated.

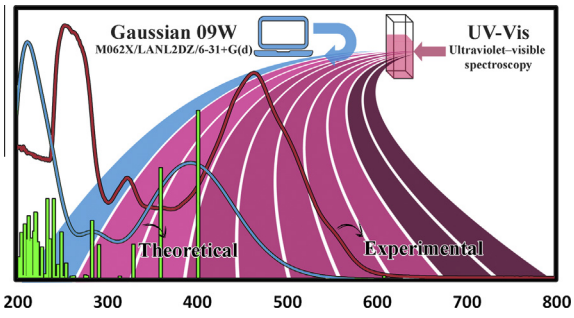

ARTICLE INFO

Article history:
Received 6 December 2014
Received in revised form 6 May 2015
Accepted 21 May 2015
Available online 30 May 2015

Keywords:
X-ray crystallography
Nickel Schiff base complexes
DFT calculation
Tridentate Schiff bases

ABSTRACT

Some new complexes of [NiL(PR_3)] (where L = (E)-1-[(2-amino-5-nitrophenyl)iminio-methyl]naphthalene-2-olate (L^1), (E)-1-[(2-hydroxiphenyl)iminio-methyl]naphthalene-2-olate (L^2), R = Bu and Ph) containing tridentate ONN and ONO Schiff bases were synthesized and characterized by IR, UV–Vis, ^{1}H-NMR spectroscopy and elemental analysis. The geometry of [NiL^1(PBu_3)] and [NiL^2(PBu_3)] complexes were determined by X-ray crystallography. It was indicated that the complexes have a square planar structure and four coordinates in the solid state. Theoretical calculations were also performed to optimize the structures of the ligands and complexes in the gas phase and ethanol solvent, separately to confirm the structures proposed by X-ray crystallography. In addition, UV–Visible and IR spectra of the complexes were calculated and compared with the corresponding experimental spectra to complete the experimental structural identification.

Introduction

The preparation of Schiff bases is easy and they can be used for synthesis of complexes with the most of metal ions in different oxidation states. Metal Schiff base complexes are investigated and

* Corresponding author. Tel.: +98 31 33913251; fax: +98 31 33912350.
E-mail addresses: akianfar@cc.iut.ac.ir, asarvestani@yahoo.com (A.H. Kianfar).

http://dx.doi.org/10.1016/j.saa.2015.05.084
1386-1425/

applied as homogeneous and heterogeneous catalysts in many areas of chemistry such as hydrogenation of olefins [1,2], transformation of amino groups [3] and oxidation of alcohols [4,5]. With the goal of structural studies and catalysis applications, tridentate Schiff base complexes containing N, O and S donor atoms have been studied in literature. They have used to prepare organic compounds by heck reaction [6]. Metal complexes containing tridentate Schiff bases and phosphine ligand are applied as catalyst in Suzuki–Miyaura cross coupling reaction [7–11]. These compounds also are applicable as collection of toxic metal [12] and inhibitor for corrosion of metals in acidic media [13].

In this work, the synthesis of some new Ni(II) Schiff base compounds containing tridentate ONO and ONN Schiff base ligands and phosphines (Scheme 1) were reported. The synthesized complexes were identified by IR, NMR, UV–Vis spectroscopy and elemental analysis techniques. The structures of $[NiL^1(PBu_3)]$ and $[NiL^2(PBu_3)]$ were determined via X-ray crystallography. In addition to experimental identifications, theoretical calculations were employed to complete and confirm the experimental observations. For this purpose, the structures of compounds were determined by theoretical calculations. The optimized molecular geometries of ligands were used to estimate their thermodynamic and kinetic parameters for their tautomeric processes. The optimized structures of complexes were compared with X-ray data and used for calculating the IR and UV–Vis spectra of complexes. Comparison of the calculated spectra, especially UV–Vis spectra, with the corresponding experimental spectra could be used as another useful tool for structural identification.

Experimental

Chemicals and apparatus

All chemicals and solvents, being of reagent quality, were used without further purification. Infrared spectra (KBr disks) were recorded on a FT-IR JASCO-68O spectrophotometer in the 4000–400 cm^{-1}. The elemental analyses were determined on a CHN-O-Heraeus elemental analyzer. UV–Vis spectra were recorded on a JASCO V-570 spectrophotometer in the 190–900 nm. The ^1H NMR spectra were recorded in $CDCl_3$ on DPX-400 MHz FT-NMR.

Synthesis

As mentioned in literature [14], the tridentate Schiff base ligand L^1 and L^2 was synthesized by adding 2-hydroxy-1-naphthaldehyde to appropriate amount of amines in methanol by 1:1 mol ratio. The solution was refluxed with stirring for 3 h. The light red precipitate was appeared during the reaction. The ligands were recrystallized from dichloromethane/methanol mixed solvents.

L^1: Yield (80%). $C_{17}H_{13}N_3O_3$: FT-IR (K Br cm^{-1}) ν_{max}, 3346 and 3472 (NH_2), 1628 (C=N), 1488 (C=C), 1316 (NO_2), 1173 (C–O). UV–Vis, λ_{max} (nm) (Ethanol): 230, 324, 389. H^1 NMR ($CDCl_3$, δ, ppm) 4.80 (s, 2H, NH_2), 6.80–8.40 (m, 9H, aromatic), 9.63 (s, 1H, HC=N), 14.43 (s, 1H, OH).

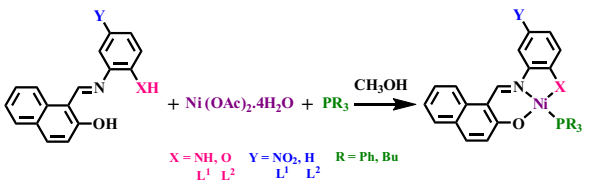

Scheme 1. The structure of Schiff bases and their complexes.

L^2: Yield (80%). $C_{17}H_{13}NO_2$: FT-IR (KBr cm^{-1}) ν_{max}, 3451 (OH), 1630 (C=N), 1547 (C=C), 1141 (C–O). UV–Vis, λ_{max} (nm) (Ethanol): 267, 334, 459. H^1 NMR ($CDCl_3$, δ, ppm) 9.49 (s, 1H, HC=N), 6.70–8.30 (m, 23H, Aromatic).

The $[NiLPR_3]$ complexes were synthesized by the following procedure. One mmol of the Schiff base ligand was added to a methanolic solution containing nickel(II) acetate and phosphine. The solution was refluxed for 2 h. During the reaction, the color of solution was changed to red brown. The solution was filtered and the brown crystals were collected after 24–48 h, washed with methanol and recrystallized from dichloromethane/methanol.

$NiL^1(PBu_3)$: Yield (80%). Anal. Calc. for $C_{29}H_{38}N_3NiO_3P$: C, 61.51%; H, 6.76%; N, 7.42%. Found; C, 62.08%; H, 7.14%; N, 7.64%. FT-IR (KBr cm^{-1}) ν_{max}, 3389 (N–H), 2955, 2927, 2869 (CH (PBu_3)), 1585 (C=N), 1479 (C=C), 1263 (NO_2), 1158 (C–O). UV–Vis, λ_{max} (nm) (Ethanol): 237, 321, 466. H^1 NMR ($CDCl_3$, δ, ppm) 0.98–1.01 (t, 9H, CH_3 of PBu_3, J = 14.8), 1.53–1.82 (m, 18H, CH_2 of PBu_3), 2.19 (s, 1H, NH), 6.46–6.48 (d, 1H, Aromatic, J = 9), 6.98–7.00 (d, 1H, Aromatic, J = 9), 7.35–7.38 (t, 1H, Aromatic, J = 14), 8.34–8.36 (d, 1H, Aromatic, J = 8), 8.75–8.76 (d, 1H, Aromatic, J = 2) and 9.78–9.81 (d, 1H, HC = N, J = 11).

$NiL^2(PBu_3)$: Yield (80%). Anal. Calc. for $C_{29}H_{38}NNiO_2P$: C, 66.69%; H, 7.33%; N, 2.68%. Found; C, 67.34%; H, 7.43%; N, 2.75%. FT-IR (KBr cm^{-1}) νmax, 2950, 2923, 2867 (CH (PBu_3)), 1613 (C=N), 1405 (C=C), 1093 (C–O). UV–Vis, λ_{max} (nm) (Ethanol): 332, 435, 460. H^1 NMR ($CDCl_3$, δ, ppm) 0.97–1.00 (t, 9H, CH_3 of PBu_3, ^3J = 14), 1.73–1.83 (m, 18H, CH_2 of PBu_3), 6.64–8.26 (m, 10H, Aromatic) and 9.52–9.55(d, 1H, HC=N, J = 11).

$NiL^1(PPh_3)$: Yield (80%). Anal. Calc. for $C_{35}H_{26}N_3NiO_3P$: C, 67.12%; H, 4.18%; N, 6.71%. Found; C, 66.18%; H, 4.37%; N, 6.81%. FT-IR (KBr cm^{-1}) ν_{max}, 3370 (N–H), 3046 CH (PPh_3), 1586 (C=N), 1435 (C=C), 1277 (NO_2), 1158 (C–O). UV–Vis, λ_{max} (nm) (Ethanol): 257, 329, 456, 528. H^1 NMR ($CDCl_3$, δ, ppm) 2.19 (s, 1H, NH), 6.19–6.21 (d, 1H, Aromatic, J = 9), 6.63–6.65 (d, 1H, Aromatic, J = 9), 7.35–7.91 (m, 20H, Aromatic), 8.79–8.79 (d, 1H, Aromatic, J = 2), 8.35–8.37 (d, 1H, Aromatic, J = 8) and 9.78–9.81 (d, 1H, HC=N, J = 11).

$NiL^2(PPh_3)$: Yield (80%). Anal. Calc. for $C_{35}H_{26}NNiO_2P$: C, 72.20%; H, 4.50%; N, 2.41%. Found; C, 73.13%; H, 4.31%; N, 2.49%. FT-IR (KBr cm^{-1}) ν_{max}, 3046 (CH (PPh_3)), 1613 (C=N), 1431 (C=C), 1099 (C–O). UV–Vis, λ_{max} (nm) (Ethanol): 330, 443, 487. H^1 NMR ($CDCl_3$, δ, ppm) 5.30–8.20 (m, 25H, Aromatic) and 9.46 (s, 1H, HC=N).

Crystal data collection and processing of $[NiL^1(PBu_3)]$ and $[NiL^2(PBu_3)]$

The X-ray diffraction measurements were made on an STOE IPDS II diffractometer with fine-focus sealed tube Graphite monochromator.

A red brown crystal with a dimension of 0.24 × 0.22 × 0.20 mm^3 for $[NiL^1(PBu_3)]$ was selected and fixed on a glass fiber and applied for data collection. Cell constants and an orientation matrix for data collection were obtained by least-squares refinement of diffraction data from 19379 unique reflections. Data were collected at a temperature of 298(2) K to a maximum 2θ value of 58.4° in a series of ω scans and 1° oscillations.

For $[Ni(L^2)(PBu_3)]$ a red brown crystal with a dimension of 0.50 × 0.49 × 0.48 mm^3 was picked out and located on a glass fiber and applied for data collection. Cell constants and an orientation matrix for data collection were achieved by least-squares refinement of diffraction data from 29052 unique reflections. Data were collected at a temperature of 120(2) K to a maximum 2θ value of 58.4° in a series of m scans and 1° oscillations.

They were integrated using the Stoe X-AREA [15] software package. The numerical absorption coefficient, i, for Mo Kα radiation was 0.71073 Å. A numerical absorption correction was applied

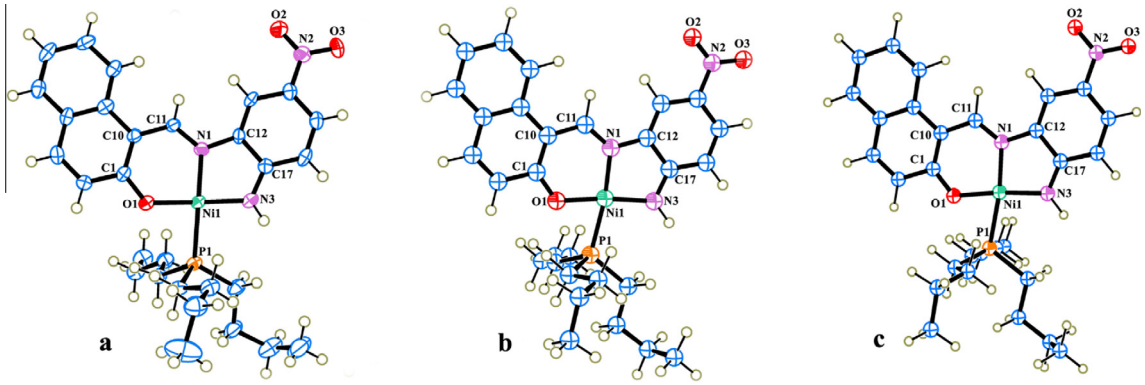

Fig. 1. The labeled diagram of [NiL^1(PBu$_3$)] showing 50% probability thermal ellipsoids in solid state, (b) the optimized structures of (a) [NiL^1(PBu$_3$)] calculated at the M062X/LANL2DZ/6-31G(d) in gas phase, (c) the optimized structures of (a) [NiL^1(PBu$_3$)] calculated at the M062X/LANL2DZ/6-31G(d) in liquid phase.

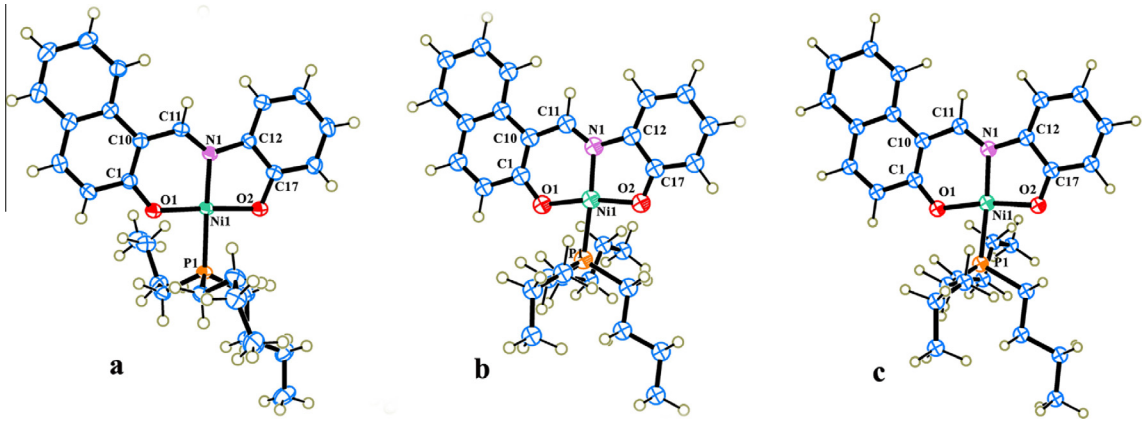

Fig. 2. The labeled diagram of [NiL^2(PBu$_3$)] showing 50% probability thermal ellipsoids in solid state, (b) the optimized structures of (a) [NiL^2(PBu$_3$)] calculated at the M062X/LANL2DZ/6-31G(d) in gas phase, (c) the optimized structures of (a) [NiL^2(PBu$_3$)] calculated at the M062X/LANL2DZ/6-31G(d) in liquid phase.

Table 1
Crystallographic and structure refinements data for [Ni(L^1)(PBu$_3$)] (A) and [Ni(L^2)(PBu$_3$)] (B).

Compound	(A)	(B)
Formula	$C_{29}H_{38}N_3NiO_3P$	$C_{29}H_{38}N\ NiO_2P$
Formula weight	566.28	522.26
Temperature/K	298	120
Wavelength λ/Å	0.71073	0.71073
Crystal system	Monoclinic	Monoclinic
Space group	$P2_1/n$	$C2/c$
Crystal size/mm^3	0.24 × 0.22 × 0.20	0.50 × 0.49 × 0.48
a/Å	14.1513 (7)	26.772 (5)
b/Å	11.0041 (5)	10.174 (2)
c/Å	18.8141 (10)	19.844 (4)
α/°	90	90
β/°	104.535 (4)	101.89 (3)
γ/°	90	90
Density (calc.)/g cm^{-3}	1.326	1.312
Z	4	8
θ ranges for data collection	2.4–29.2	2.46–29.15
F(000)	1200	2224
Absorption coefficient	0.775	0.820
Index ranges	$-19 \leqslant h \leqslant 19$ $-15 \leqslant k \leqslant 13$ $-25 \leqslant l \leqslant 25$	$-36 \leqslant h \leqslant 36$ $-13 \leqslant k \leqslant 13$ $-27 \leqslant l \leqslant 25$
Data collected	19379	29052
Unique data (R_{int})	7596, (0.100)	7112, (0.054)
Parameters, restrains	334, 0	310, 0
Final R$_1$, wR_2^a (obs. data)	0.085, 0.136	0.0382, 0.0864
Final R$_1$, wR_2^a (all data)	0.0998, 0.1359	0.0483, 0.0900
Goodness of fit on F^2 (S)	1.01	1.059
Largest diff peak and hole/e Å^3	0.46, −0.42	0.340, −0.533

using X-RED [16] and X-SHAPE [17] softwares. The data were corrected for Lorentz and polarizing effects. The structures were solved by direct methods [18]. The subsequent difference Fourier maps were then refined on F^2 by a full-matrix least-squares procedure using anisotropic displacement parameters [19]. H atoms were positioned geometrically and constrained to ride on their parent atoms.

The NH hydrogen atom was located in a difference Fourier map and then refined isotropically. Atomic factors are from International Tables for X-ray Crystallography [20]. All refinements were performed using the X-STEP32 crystallographic software package [21].

Computational details

The structures of the synthesized ligands and complexes were studied using density functional theory (DFT) employing M062X functional. The 6-31+G(d) basis set was selected for C, N, O, P and H atoms. In addition, the standard relativistic effective core pseudo potential LANL2DZ was used for Ni atom. The structures of the considered ligands were optimized only in the gas phase and the structures of complexes were optimized in both gas and ethanol solvent. The polarized continuum model (PCM) was used for modeling the solvent in our calculations. In this model, only the electrostatic field of solvent was considered. The IR spectra of the optimized structures of complexes in the gas phase were calculated using the same functional and basis set. The time dependent density function theory (TD-DFT) method with the same functional

Table 2
Selected bond distances (Å) and bond angles (°) for [NiL^1(PBu$_3$)] (A), [NiL^2(PBu$_3$)] (B), from X-ray analysis and Gousian09 calculations at the M062X/6-31+g(d) method in gas phase and M062X/6-31+g(d)/LANL2DZ method in liquid phase for both complexes.

	(A)			(B)		
	X-ray	Gas phase	Liquid phase	X-ray	Gas phase	Liquid phase
Bond distances						
N1–Ni1	1.880 (4)	1.891 (35)	1.900 (41)	1.871 (4)	1.877 (18)	1.882 (27)
N3–Ni1	1.844 (3)	1.889 (11)	1.884 (97)	–	–	–
O1–Ni1	1.837 (3)	1.829 (69)	1.826 (28)	1.822 (3)	1.817 (47)	1.812 (92)
Ni1–P1	2.186 (4)	2.171 (10)	2.174 (47)	2.183 (6)	2.159 (48)	2.164 (89)
C1–O1	1.313 (5)	1.306 (24)	1.301 (83)	1.306 (6)	1.307 (88)	1.307 (03)
C1–C10	1.402 (6)	1.409 (51)	1.412 (40)	1.413 (2)	1.411 (53)	1.411 (89)
C10–C11	1.425 (5)	1.448 (33)	1.445 (70)	1.423 (2)	1.452 (86)	1.450 (83)
C11–N1	1.315 (4)	1.308 (76)	1.310 (62)	1.307 (2)	1.305 (58)	1.306 (87)
C12–N1	1.408 (5)	1.425 (58)	1.427 (82)	1.412 (2)	1.418 (57)	1.420 (26)
C12–C17	1.429 (5)	1.462 (97)	1.475 (24)	1.409 (2)	1.437 (61)	1.436 (10)
C17–N3	1.327 (6)	1.339 (64)	1.325 (58)	–	–	–
N3–H3A	0.860	1.014 (55)	1.021 (94)	–	–	–
C18–P1	1.821 (4)	1.897 (66)	1.889 (99)	1.823 (5)	1.896 (78)	1.892 (67)
C22–P1	1.817 (4)	1.891 (72)	1.889 (65)	1.821 (7)	1.893 (60)	1.890
C26–P1	1.824 (4)	1.892 (40)	1.889 (44)	1.823 (5)	1.891 (11)	1.888 (91)
C14–N2	1.412 (6)	1.445 (63)	1.412 (20)	–	–	–
N2–O2	1.236 (4)	1.227 (87)	1.239 (52)	–	–	–
N2–O3	1.243 (4)	1.226 (49)	1.238 (65)	–	–	–
O2–Ni1	–	–	–	1.842 (7)	1.838 (02)	1.839 (59)
C17–O2	–	–	–	1.331 (1)	1.313 (13)	1.315 (65)
Bond angles						
N3–Ni1–P1	95.5 (9)	100.1 (27)	100.3 (79)	–	–	–
O1–Ni1–P1	85.6 (4)	73.8 (45)	74.1 (99)	86.32 (4)	76.9 (40)	76.6 (41)
O1–Ni1–N1	94.5 (7)	98.3 (33)	97.9 (38)	95.14 (6)	99.5 (65)	99.0 (71)
N3–Ni1–N1	84.7 (2)	87.6 (93)	87.4 (87)	–	–	–
N1–Ni1–P1	174.6 (0)	172.1 (79)	172.1 (20)	177.03 (4)	176.4 (71)	175.6 (68)
O1–Ni1–N3	174.4 (1)	173.9 (72)	174.5 (51)	–	–	–
C17–N3–Ni1	115.9 (3)	111.7 (77)	112.3 (08)	–	–	–
Ni1–N3–H3A	122.0	129.9 (41)	128.7 (92)	–	–	––
C11–N1–Ni1	126.3 (3)	125.0 (62)	125.2 (20)	125.87 (1)	125.3 (71)	125.6 (66)
C12–N1–Ni1	112.8 (2)	111.0 (50)	111.0 (96)	110.83 (1)	108.2 (92)	108.5 (17)
C1–O1–Ni1	127.2 (3)	123.1 (12)	123.4 (46)	127.37 (1)	121.6 (73)	122.1 (99)
C18–P1–Ni1	116.2 (9)	115.8 (29)	115.7 (60)	116.59 (6)	114.5 (04)	114.1 (61)
C22–P1–Ni1	113.2 (4)	112.8 (55)	112.4 (52)	108.28 (6)	112.3 (50)	111.9 (69)
C26–P1–Ni1	111.5 (9)	112.8 (29)	112.4 (32)	115.11 (6)	114.0 (41)	113.8 (09)
O2–Ni1–P1	–	–	–	90.85 (4)	92.8 (14)	93.9 (73)
O2–Ni1–N1	–	–	–	87.59 (6)	90.6 (78)	90.3 (11)
O1–Ni1–O2	–	–	–	176.48 (5)	169.7 (54)	170.6 (14)
C17–O2–Ni1	–	–	–	111.33 (1)	108.4 (49)	108.7 (80)
O1–C1–C10	125.9 (4)	127.8 (58)	127.9 (79)	125.42 (14)	128.5 (43)	128.4 (62)
C1–C10–C11	120.9 (3)	122.7 (66)	122.7 (13)	120.76 (14)	122.9 (86)	122.9 (04)
N1–C11–C10	124.9 (4)	122.8 (65)	122.6 (52)	125.19 (14)	121.8 (53)	121.6 (94)
N1–C12–C17	112.0 (4)	112.2 (68)	111.5 (78)	111.66 (13)	111.5 (63)	111.5 (78)
C11–N1–C12	120.8 (4)	123.8 (87)	123.6 (82)	123.17 (13)	126.3 (36)	123.6 (82)
N3–C17–C12	114.5 (3)	117.2 (09)	117.5 (23)	–	–	–
O2–C17–C12	–	–	–	118.48 (14)	121.0 (14)	120.9 (04)

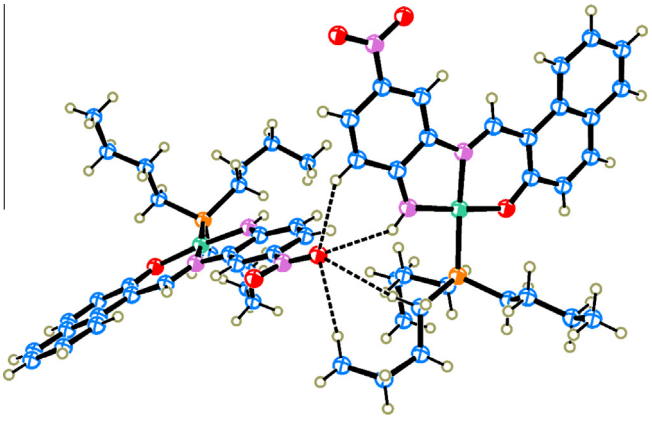

Fig. 3. A view of the extended network of complex [NiL^1(PBu$_3$)] with the intermolecular hydrogen bonds showing 50% probability thermal ellipsoids (dashed black lines).

and basis set was used for calculating the UV–Vis spectra of the complexes in the ethanol using the optimized structures of complexes in the solvent. The tautomerism processes of the synthesized ligands were also studied computationally in this work using two different levels of theory including DFT (M062X functional) and MPWLYP methods in the gas phase. QST2 method was used to obtain the transition states structures connecting enol to keto-imine. All of the calculations were performed using Gaussian 2009 software [22].

Results and discussion

IR spectra

The IR spectral data are shown in the experimental section. L^1 and L^2 show a sharp peak in the region of 1628 and 1630 cm^{-1}, respectively characteristic of the azomethine group. This band shifts to the low frequencies relative to the free ligands after coordination of the Schiff bases to Ni(II) ion. The phenolic (OH)

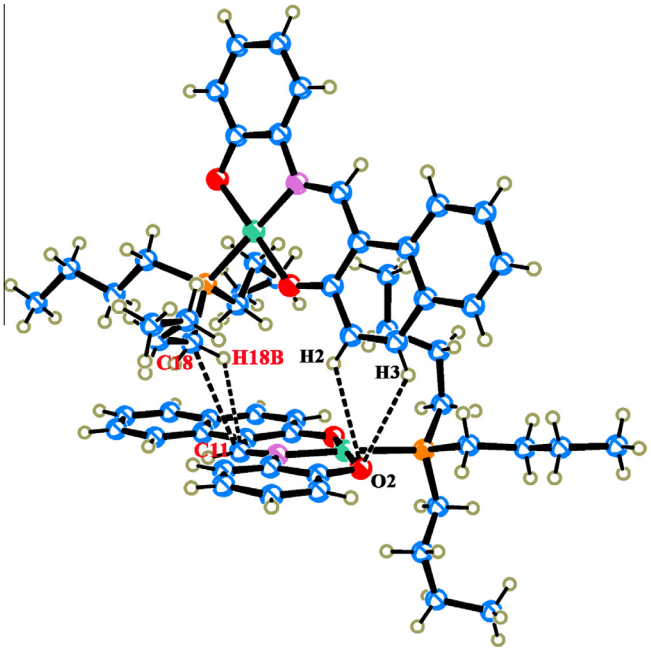

Fig. 4. A view of the extended network of complex [NiL^2(PBu$_3$)] with the intermolecular interactions showing 50% probability thermal ellipsoids (dashed black lines).

Table 3
Significant bond lengths and bond angles calculated at the mpw2plyp/6-31+g(d) level for H_2L^1 and M062x/6-31+g(d) level for H_2L^2.

Structural parameter	H_2L^1			H_2L^2		
	A-1	TS_1	A-2	B-1	TS_2	B-2
Bond lengths (Å)						
C1–O1	1.34	1.30	1.26	1.33	1.28	1.25
C1–C10	1.40	1.43	1.46	1.41	1.43	1.46
C10–C11	1.44	1.41	1.39	1.44	1.41	1.39
C11–N1	1.30	1.31	1.33	1.29	1.30	1.34
N1–C12	1.40	1.40	1.40	1.40	1.39	1.40
C12–C17	1.42	1.41	1.41	1.41	1.40	1.41
C17–N3	1.37	1.37	1.37	–	–	–
C17–O2	–	–	–	1.36	1.35	1.36
N1–H1	1.71	1.22	1.03	1.66	1.22	1.03
O2–H2	–	–	–	0.96	0.96	0.96
O1–H1	0.99	1.24	1.69	1.00	1.25	1.74
N3–H1N3	1.00	1.01	1.01	–	–	–
N3–H2N3	1.00	1.00	1.00	–	–	–
Bond angles (°)						
C1–O1–H1	107.98	103.99	104.314	107.55	104.73	107.55
C1–C10–C11	119.92	117.16	118.55	119.29	116.76	118.65
C10–C11–N1	122.95	120.21	123.42	122.09	120.07	124.43
C11–N1–C12	119.83	123.92	126.33	121.90	125.17	127.38
N1–C12–C17	117.05	117.39	117.43	117.44	116.73	116.78
C12–C17–O2	–	–	–	117.12	116.27	116.08
C12–C17–N3	119.68	120.17	120.21	–	–	–
C17–O2–H2	–	–	–	108.73	110.30	109.69
C17–N3–H1N3	117.12	118.24	118.64	–	–	–
C17–N3–H2N3	117.78	117.41	116.70	–	–	–
C10–C1–O1	122.95	121.25	122.48	123.05	121.79	122.70

vibration peak is seen in the 2500–3500 cm^{-1} region. This band disappears after coordination of ligands to the metal ion. For L^1 ligand the NH_2 stretching frequencies are seen at 3346 and 3472 cm^{-1} while the symmetry vibrational frequency of NO_2 is seen at 1316 cm^{-1}. In the complexes containing L^1, the N–H vibration appears at about 3370–3389 cm^{-1} region as a single peak which shows that the NH_2 functional group has been changed to NH after coordination of Schiff base ligand. The NO_2 stretching frequency of L^1 complexes is seen at the range of 1263–1277 cm^{-1}. The complexes containing PBu_3 show the C–H vibration frequencies at about 2867–2954 cm^{-1} and the peaks at about 3046 cm^{-1} are related to the aromatic C–H vibration of complexes containing PPh_3.

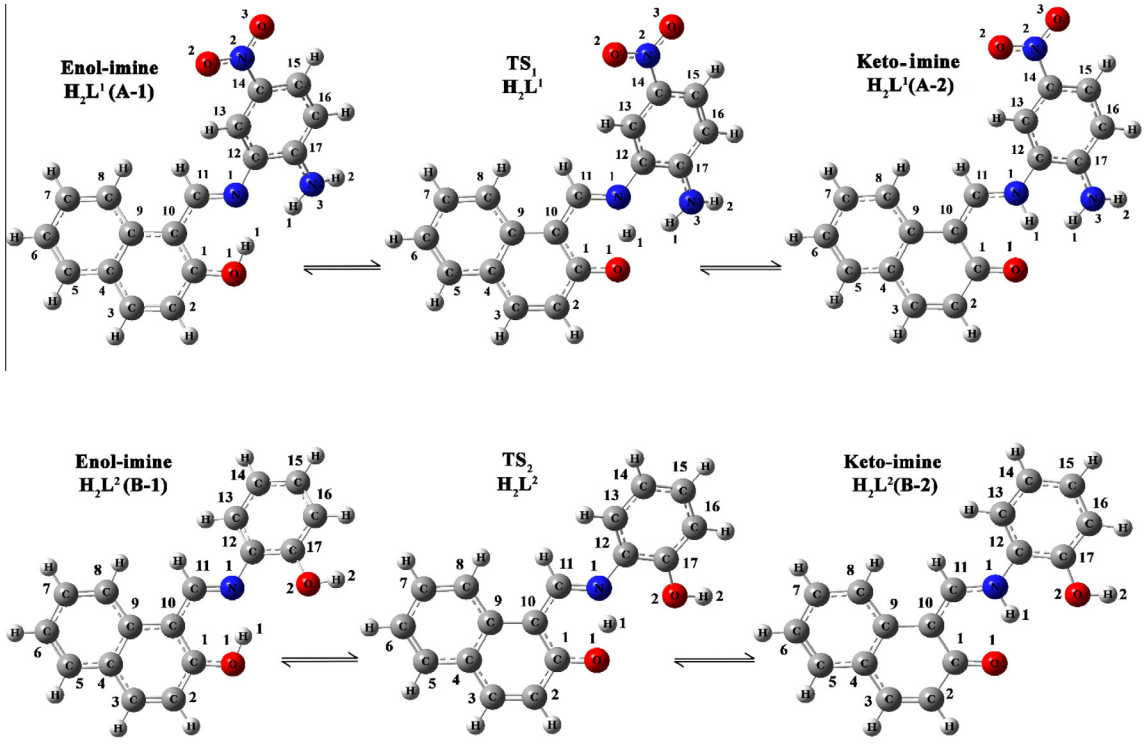

Fig. 5. Optimized structures of H_2L^1 and H_2L^2.

Table 4
Relative energies ΔE (kJ mol^{-1}), zero point energies ZPE (kJ mol^{-1}) and dipole moments μ (D) of the isomers of ligands calculated at the mpw2plyp method for H_2L^1 and M062x method for H_2L^2 using a 6-31+g(d) basis set.

H_2L^1	ΔE	ZPE	μ	Freq
A-1	0.0	722.76	6.58	–
TS_1	22.33	710.82	5.71	−1315.5
A-2	7.89	723.34	4.83	–
H_2L^2	ΔE	ZPE	μ	Freq
B-1	0.0	680.84	2.25	–
TS_2	18.62	675.40	2.91	−1176.3
B-2	3.4	684.93	3.41	–

Table 5
Activation energy for forward reaction $E_{a,f}$ (kJ mol^{-1}), activation energy for reverse reaction $E_{a,r}$ (kJ mol^{-1}), standard free energy for forward reaction $\Delta G^{\neq}_f$ (kJ mol^{-1}), standard free energy for reverse reaction $\Delta G^{\neq}_r$ (kJ mol^{-1}), kinetic rate constant for forward reaction k_f and kinetic rate constant for reverse reaction k_r for R_1 and R_2 reactions.

Energy	R_n	
	R_1	R_2
$E_{a,f}$	10.39	9.34
$E_{a,r}$	1.92	5.69
$\Delta G^{\neq}_f$	10.696	6.277
$\Delta G^{\neq}_r$	4.818	4.485
k_f	8.31×10^7	4.95×10^8
k_r	8.91×10^8	1.02×10^9

Electronic spectra

The electronic absorption spectra of all Schiff base ligands and synthesized complexes in ethanol solution showed the bands in the 200–600 nm regions. The electronic spectra of the Schiff bases consisted of relatively intense bands in the 250–350 nm region, involving transition of aromatic rings [23]. These bands were seen in the range of 250–334 nm for the coordinated ligands. The azomethine $\pi \rightarrow \pi^*$ transition band for L^1 and L^2 appeared at 389 and 459 nm, respectively. The intense bands in the range of 400–530 nm, were corresponded to $\pi \rightarrow \pi^*$ azomethine and $d \rightarrow \pi^*$ transition [24,25]. The absence of electronic transition higher than 600 nm wavelengths indicates a large crystal-field splitting and is accompanied by the square planar geometry of Ni(II) complexes [26,27].

^{1}H NMR spectra

The ^{1}H NMR spectral data for [NiL(PR_3)] complexes in $CDCl_3$ solvent are given in section "Synthesis". The peaks related to tributylphosphine were seen as triplet for CH_3 and multiplet for CH_2 groups in the range of 0.98–1.01 ppm and 1.53–1.82 ppm, respectively. The NH signal was appeared at 2.19 and 2.18 ppm for $NiL^1(PBu_3)$ and $NiL^1(PPh_3)$ complexes, respectively. The aromatic hydrogens of Schiff base ligands and triphenylphosphine were assigned in the range of 6.40–9.00 ppm. The imine hydrogen (HC=N) was splitted by phosphine and appeared as a doublet signal at about 9.40–9.80 ppm in the synthesized complexes [13,27].

Table 6
Atomic charges (e) calculated from natural population analysis.

Atom	Compound		
	A-1	A-2	$NiL^1(PBu_3)$
O(1)	−0.730	−0.672	−0.391
N(1)	−0.344	−0.539	−0.107
N(3)	−0.903	−0.852	−0.508
P(1)	–	–	3.186
Ni(1)	–	–	−0.041
	B-1	B-2	$NiL^2(PBu_3)$
O(1)	−0.666	−0.584	−0.332
N(1)	−0.315	−0.498	−0.154
O(2)	−0.642	−0.703	−0.220
P(1)	–	–	3.213
Ni(1)	–	–	−0.495

Description of the molecular structure of [$NiL^1(PBu_3)$] and [$NiL^2(PBu_3)$]

The structure of [$NiL^1(PBu_3)$] and [$NiL^2(PBu_3)$] complexes were determined by X-ray diffraction. The ORTEP representations are shown in Figs. 1 and 2. X-ray diffraction data and the selected bond lengths and angles were listed in Tables 1 and 2.

The [$NiL^1(PBu_3)$] complex was crystallized in the monoclinic space group $P2_1/n$. According to the crystal structure, the [$NiL^1(PBu_3)$] was contained tridentate ONN Schiff base and a monodentate tributylphosphine ligand. The nickel atom had an approximate square planar coordinate with O1, N1, N3 of Schiff base and P1 of tributylphosphine with a metal atom having the maximum deviation of 0.004 Å from the mean plane. The angles O(1)–Ni(1)–N(3) = 174.41 (17)°, N(1)–Ni(1)–P(1) = 174.6 (01), O1–Ni1–P1 = 85.64 (10)°, N1–Ni1–N3 = 84.72 (15)°, N(3)–Ni(1)–P(1) = 95.59 (12)° and O1–Ni1–N1 = 94.57 (13)° indicated that the coordination geometry of the nickel atom distorted from the square planar. The Ni–O, Ni–N and Ni–P distances of 1.837 (3) Å, 1.880 (4) Å, 1.844 (3) Å and 2.1864 (13) Å for Ni(1)–O(1), Ni(1)–N(1), Ni(1)–N(3) and Ni(1)–P(1), respectively were in the ranges observed for analogous compounds of nickel square planar complexes containing tridentate Schiff bases and phosphine ligands [7,8,27].

The bond distances of coordinated nitrogens with carbons were increased in the trend of N1–C11(1.315) < N3–C17(1.327) < N3–C12(1.408). The bond order of N1–C11 and N1–C12 is double and single, respectively. The bond length of N3–C17 is in the range of

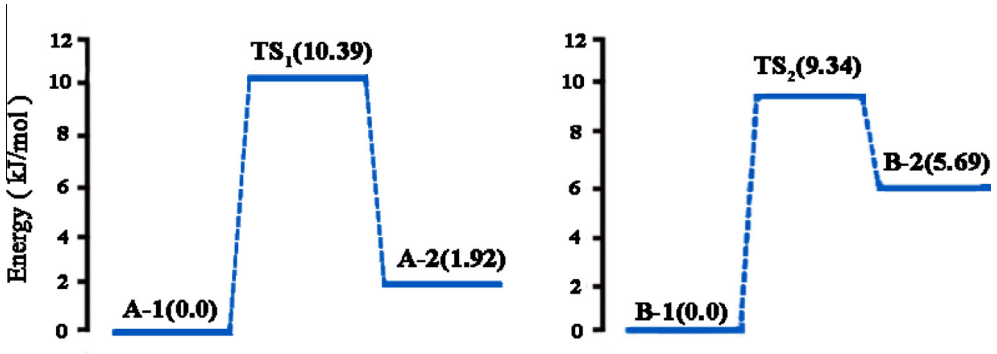

Fig. 6. Relative energies of different species for reaction R1 and R2 in kJ mol^{-1} at the mpw2plyp/6-31+g(d) for TS_1 and the M062X/6-31+g(d) for TS_2.

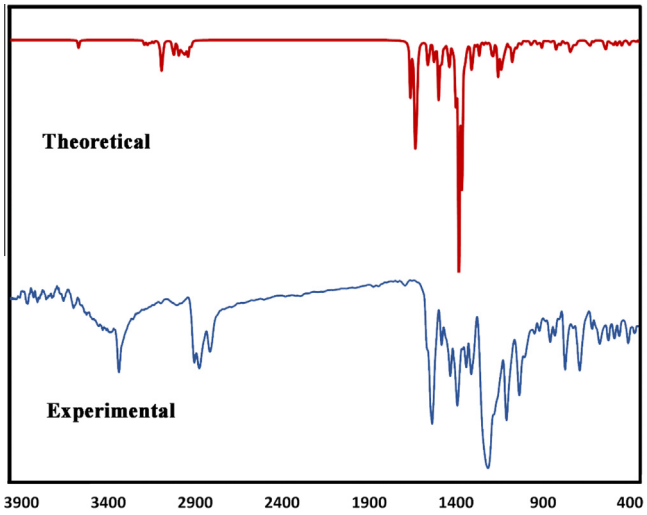

Fig. 7. The experimental and theoretical IR spectra of [NiL^1(PBu$_3$)].

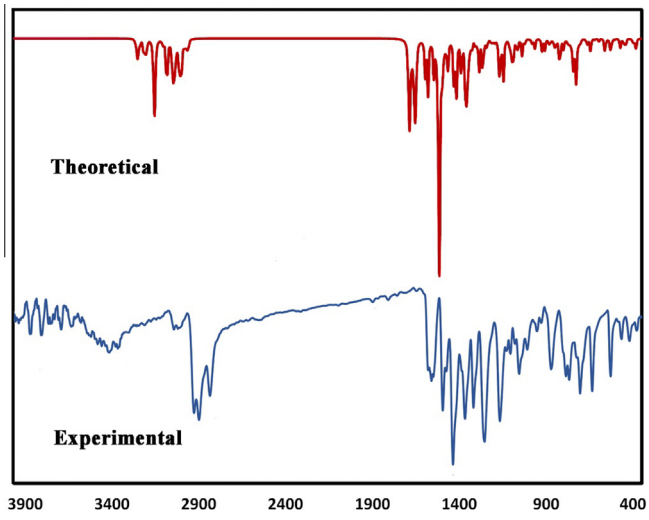

Fig. 8. The experimental and theoretical IR spectra of [NiL^2(PBu$_3$)].

carbon nitrogen double bond. This is due to the participation of the N3 lone pair in resonance with aromatic ring [23,27].

In contrast to the similar Ni(II) Schiff base complexes containing the PPh_3 [27], according to the Fig. 3, [NiL^1(PBu$_3$)] complex shows strong and short hydrogen bonding between the N–H and the NO_2 functional group which lead to stabilization of the lattice. The N3–H3A hydrogen is bonded to O3–N2 of NO_2 functional group (N3–H3A···O3–N2 (2.481)). Also the NO_2 group is bonded to H16 (O3–H16, 2.685), H21B(O3–H21B, 2.680) and H27A(O2–H27A, 2.692) via hydrogen bonding.

The [NiL^2(PBu$_3$)] complex was crystallized in the monoclinic space group *C2/c*. The [NiL^2(PBu$_3$)] was contained tridentate ONO Schiff base and a monodentate tributylphosphine ligand. The nickel atom had an approximate square planar coordinate with O1, N1, O2 of Schiff base and P1 of tributylphosphine are showed the maximum deviation of 0.04 Å from the mean plane. The angles O(1)–Ni(1)–O(2) = 176.48 (5)°, N(1)–Ni(1)–P(1) = 177.03 (4), O1–Ni1–P1 = 86.32 (4)°, O1–Ni1–N1 = 95.14 (6)°, O(2)–Ni(1)–N(1) = 87.59 (6)° and O2–Ni1–P1 = 90.85 (4)° with a distorted square planar geometry for the Ni atom. The Ni–O, Ni–N and Ni–P distances of 1.822 (31) Å, 1.871 (41) Å, 1.842 (71) Å and 2.183

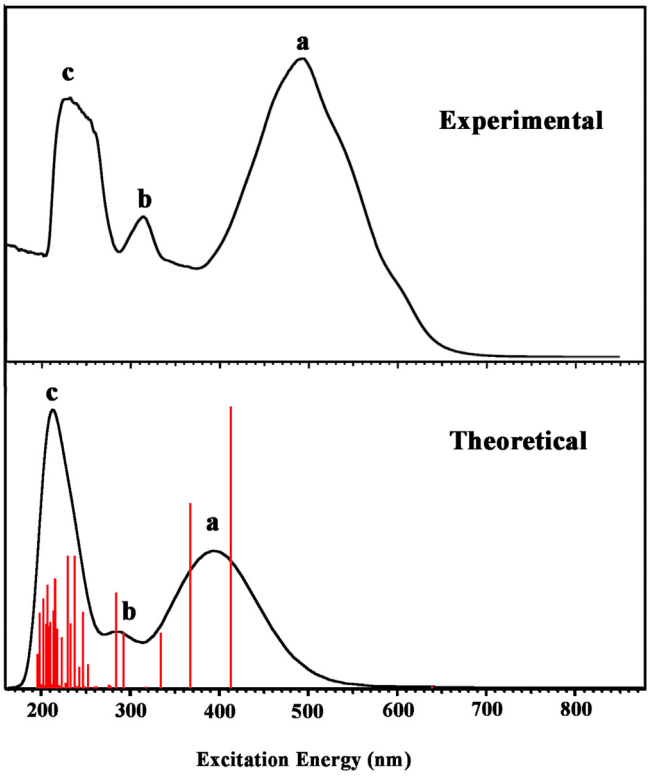

Fig. 9. The experimental and theoretical electronic spectra of [NiL^1(PBu$_3$)] (in ethanol).

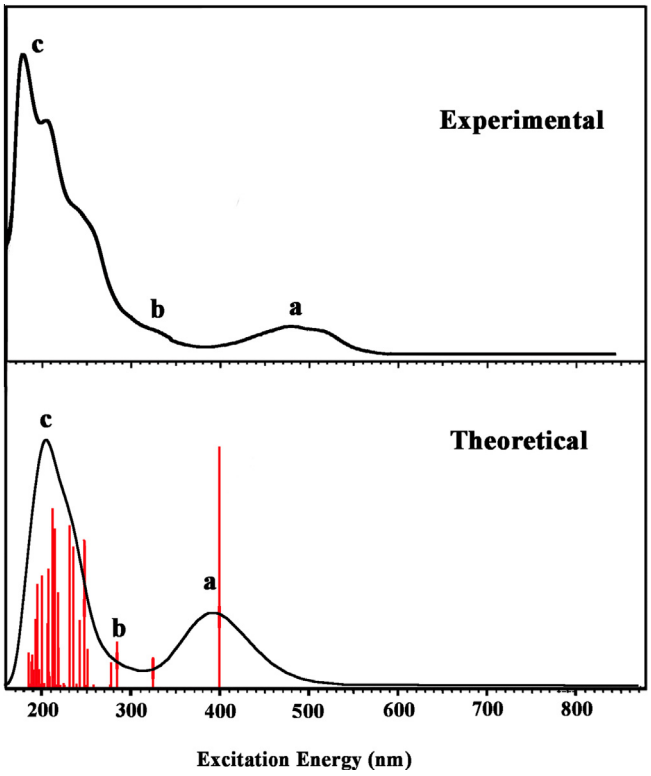

Fig. 10. The experimental and theoretical electronic spectra of [NiL^2(PBu$_3$)] (in ethanol).

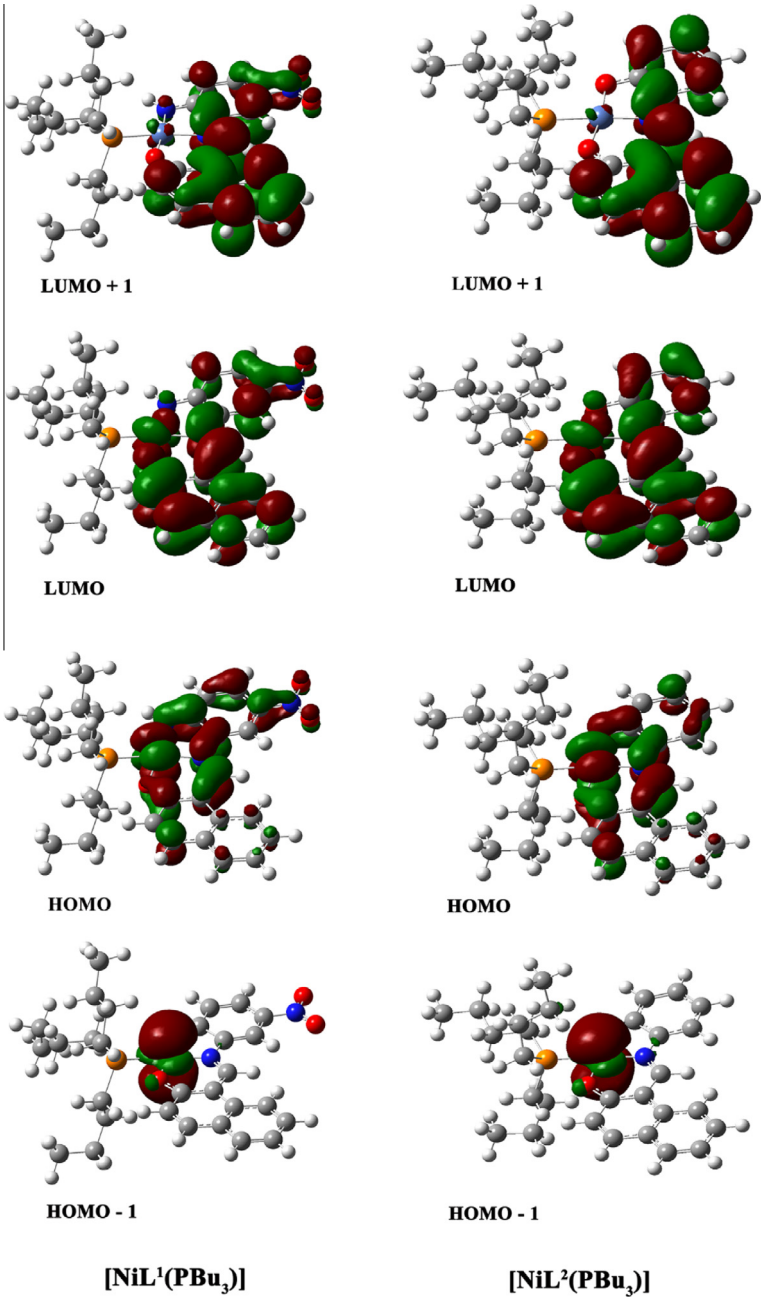

Fig. 11. The shapes of the molecular orbitals of $[NiL^1(PBu_3)]$ and $[NiL^2(PBu_3)]$ complexes.

(6) Å for Ni(1)–O(1), Ni(1)–N(1), Ni(1)–O(2) and Ni(1)–P(1), respectively were in the range of reported nickel square planar complexes [26].

The short interactions lead to stabilization of the lattice in the $NiL^2(PBu_3)$ complex. Short interactions (H2–O2 (2.852), H3–O2 (3.065) and C11–H18 (2.797)) between adjacent molecules and intermolecular π–π interactions of six-membered rings (C18–C11(3.342)) stabilize the lattice (Fig. 4).

Theoretical results

Molecular structure and analysis of bonding modes of Schiff base ligands

The stability of the different tautomers of each considered ligands and their geometries are discussed in this section. Fig. 5 demonstrated the optimized geometries of the ligands in the gas phase in the forms of enol, keto-imine and their related transition states. In addition, Table 3 tabulated the significant bond lengths and bond angles of each ligand for both enol and keto-imine forms. The calculated structural data of L^1 can be compared with the corresponding experimental data reported in Ref. [14]. It can be seen that there is a good agreement between the theory and experiment which means that the structure of L^1 in solid state is very close to that in the gas phase (also see Table 4).

Table 5 reports the calculated kinetic parameters related to the tautomeric reactions shown in Fig. 5 and the related energy diagrams have been demonstrated in Fig. 6. The activation electronic energies, considering zero point energy, of forward reactions are higher than those of the reverse reactions. Table 5 also shows that the enol form of ligands are more stable than the ketoimine form based on the calculated standard activation Gibbs free energies of forward and reverse reaction. The imaginary frequency for the

transfer of proton from the oxygen atom to the nitrogen atom for L^1 and L^2 is about −1315.5 and −1176.3 cm^{-1}, respectively. The Mullikan atomic charges of the atoms involved in the tautomeric process for enol and keto-imine have been reported in Table 6. The change in the atomic charges of O1 and N1 in the tautomeric process confirms the presence of double bond between C1 and O1 in keto form and mainly the single bond between C11 and N1 atoms in keto-imine.

Molecular structure and analysis of bonding modes of complexes

The geometries of complexes are signified in Figs. 1 and 2. Some calculated bond lengths and bond angles of these two complexes, obtained from the calculation in the gas phase and ethanol, were compared with the corresponding experimental values obtained from X-ray data in Table 2. As seen in Table 2, the results show that the structural characteristics of the complexes in the solid state and gas phase are nearly similar and confirm the applied theoretical method. The main difference between experimental and theoretical structure is the distortion of the PR_3 toward naphthaldehyde rings. In both complexes the angle of O1–Ni1–P1 was decreased while N3–Ni1–P1 (in $[NiL^1(PBu_3)]$) and O1–Ni1–P1 that cause the change in bond angles of N3–Ni1–P1 and O1–Ni1–P1 (in $[NiL^2(PBu_3)]$) were increased (Table 2).

Theoretical study of IR spectra

Figs. 7 and 8 shows the comparison of the calculated and experimental IR spectra of the $[NiL^1(PBu_3)]$ and $[NiL^2(PPh_3)]$ complexes, respectively, in gas phase and solid state. The good agreement between theory and experiment is shown that there is a good similarity between the structure of the complexes in the gas phase and solid state. The calculated frequency of C=N stretching for both $[NiL^1(PBu_3)]$ and $[NiL^2(PBu_3)]$ is about 1585 and 1613 cm^{-1} which is close to the experimental values reported in section "IR spectra" (1585 and 1475 cm^{-1}). The features related to C–H stretching of coordinated PBu_3 ligand is appeared in the range of 2956–3226 cm^{-1}. The N–H vibration frequency is appeared at about 3600 cm^{-1} in theoretical calculations while the experimental data show this frequency at about 3389 cm^{-1}. Also the NO_2 stretching frequency is seen at 1408 and 1426 cm^{-1} in calculated spectra of complexes in comparison to experimental study that shows sharp peaks in 1263 and 1277 cm^{-1} region. In theoretical study the most differences have been observed for N–H and NO_2 vibrational frequencies because of N–H and NO_2 hydrogen bonding in the solid state.

Theoretical study of UV–Vis spectra

Figs. 9 and 10 compares the calculated absorption spectra of $[NiL^1(PBu_3)]$ and $[NiL^2(PBu_3)]$ in ethanol solvent, respectively. It can be seen that the calculated spectra can describe the experimental spectra relatively well. The agreement between the theory and experiment confirms the proposed structures for the synthesized complexes. Theoretical calculations show that the feature *a* in the recorded spectrum of $[NiL^1(PBu_3)]$ has been composed from three absorption bands located at 412.66, 367.1 and 334.07 nm which are related to the excitation of complex from the ground state to the fifth, sixth and seventh excited electronic states of complex, respectively. These transitions are related to the promotion of electron from HOMO → LUMO, HOMO → LUMO + 1 and HOMO − 1 → LUMO, respectively. The feature *b* has been composed from two absorption bands located at 292.3 and 283.89 nm. The line located at 292.3 nm is related to the promotion of electron from HOMO − 1 to LUMO and LUMO + 1 with nearly the same probability. As seen in the Fig. 8 feature *c* has been composed from many absorption bands close to each other. The feature 8 (centered at 391.72 nm) in the calculated spectrum of $[NiL^2(PBu_3)]$ unlike $[NiL^1(PBu_3)]$ has been composed of only one absorption band. This band is related to the promotion of electron from HOMO to LUMO.

The shapes of the molecular orbitals including HOMO-1, HOMO, LUMO and LUMO + 1 of two complexes, calculated at the DFT level of theory employing M062X functional and 6-31+G(d) basis set for C, N, O, P and H atoms and the standard relativistic effective core pseudo potential LANL2DZ, have been demonstrated in Fig. 11. It is seen that the HOMO of two complexes are mostly located on a part of L^1 and L^2 ligand (phenyl ring) and partly related to *d* orbital of metal atom. Fig. 11 shows that the HOMO − 1 of complexes is mainly related to the d_z^2 orbital of Ni atom. The LUMO and LUMO + 1 of complexes are located on only L^1 and L^2 ligands but, the contribution of metal atom is nearly zero in these orbitals.

Conclusions

In summary, $[NiL(PR_3)]$ complexes were synthesized and their structures were identified by different techniques. The FT-IR, ^1H NMR, ^{13}C NMR and X-ray crystallography results confirmed that the synthesized complexes contain Schiff base and phosphine. According to the X-ray crystallography results, the synthesized complexes were square planar and four coordinates in the solid state. Theoretical calculations of the structures of complexes, their UV–Visible and IR spectra were performed for the characterization of complexes and confirmation of experimental results.

Acknowledgements

We wish to express our gratitude to the Research Affairs Division Isfahan University of Technology (IUT), Isfahan, for financial support.

Appendix A. Supplementary data

CCDC Nos. 990831 and 888601 contains the supplementary crystallographic data for $[NiL^1(PBu_3)]$ and $[NiL^2(PBu_3)]$, respectively. These data can be obtained at www.ccdc.cam.ac.uk/deposit or from the Cambridge Crystallographic Data Center 12, Union Road Cambridge CB2 1EZ, UK; Fax: (internet) +44 1223/336 033; E. mail: deposit@ccdc.cam.ac.uk). Supplementary data associated with this article can be found, in the online version, at http://dx.doi.org/10.1016/j.saa.2015.05.084.

References

[1] R.D. Jones, D.A. Summerville, F. Basalo, Chem. Rev. 79 (1979) 139–179.
[2] S. Bhunia, S. Koner, Polyhedron 30 (2011) 1857–1864.
[3] H. Dugas, C. Penney, Bioorganic Chemistry, Springer, New York, 1981. p. 435.
[4] D. Ramakrishna, B. Ramachandra Bhat, R. Karvembu, Catalysis communications 11 (2010) 498–501.
[5] M.M. Tamizh, K. Mereiter, K. Kirchner, R. Karvembu, J. Organomet. Chem. 700 (2012) 194–201.
[6] P. Pattanayak, J.L. Pratihar, D. Patra, C.-H. Lin, S. Paul, K. Chakraborty, Polyhedron 51 (2013) 275–282.
[7] M.M. Tamizh, K. Mereiter, K. Kirchner, B.R. Bhat, R. Karvembu, Polyhedron 28 (2009) 2157–2164.
[8] M.M. Tamizh, B. Varghese, A. Endo, R. Karvembu, Spectrochim. Acta Part A Mol. Biomol. Spectrosc. 77 (2010) 411–418.
[9] S. Priyarega, M.M. Tamizh, S. Ganesh Babu, R. Karvembu, K. Natarajan, Indian J. Chem. 51A (2012) 453–457.
[10] M.M. Tamizh, K. Mereiter, K. Kirchner, R. Karvembu, J. Organomet. Chem. 700 (2012) 194–201.
[11] M.M. Tamizh, B.F.T. Cooper, C.L.B. Macdonald, R. Karvembu, Inorg. Chim. Acta 394 (2013) 391–400.
[12] W.J. Sawodny, M. Riederer, Angew. Chem. Int. Ed. Engl. 16 (1977) 859–860.
[13] M. Behpour, S.M. Ghoreishi, N. Soltani, M. Salavati-Niasari, M. Hamadanian, A. Gandomi, Corros. Sci. 50 (2008) 2172–2181.
[14] A.M. Farag, S.G. Teoh, H. Osman, S. Chantrapromm, H. Fun, Acta Cryst. E66 (2010) o1227–o1228.
[15] Stoe & Cie, X-AREA, version 1.30: Program for the Acquisition and Analysis of Data; Stoe & Cie GmbH: Darmstadt, Germany, 2005.

[16] Stoe & Cie, X-RED, Version 1.28b: Program for Data Reduction and Absorption Correction; Stoe & Cie GmbH: Darmstadt, Germany, 2005.
[17] Stoe & Cie, X-SHAPE, Version 2.05: Program for Crystal Optimization for Numerical Absorption Correction; Stoe & Cie GmbH: Darmstadt, Germany, 2004.
[18] G.M. Sheldrick, SHELX97. Program for Crystal Structure Solution, University of Göttingen, Germany, 1997.
[19] G.M. Sheldrick, SHELX97. Program for Crystal Structure Refinement, University of Göttingen, Germany, 1997.
[20] International Tables Foe X-ray Crystallography, vol. C, Kluwer Academic Publisher, Dordrecht, The Netherlands, 1995.
[21] Stoe & Cie, X-STEP32, Version 1.07b: Crystallographic Package; Stoe & Cie GmbH: Darmstadt, Germany, 2000.
[22] M.J. Frisch, H.B. Schlegel, G.W. Trucks, G.E. Scuseria, M.A. Robb, J.R. Cheeseman, 640 G. Scalmani, V. Barone, B. Mennucci, G.A. Petersson, H. Nakatsuji, M. Caricato, 641 X. Li, H.P. Hratchian, A.F. Izmaylov, J. Bloino, G. Zheng, J.L. Sonnenberg, M. 642 Hada, M. Ehara, K. Toyota, R. Fukuda, J. Hasegawa, M. Ishida, T. Nakajima, Y. 643 Honda, O. Kitao, H. Nakai, T. Vreven, J.A. Montgomery, Jr., J.E. Peralta, F. Ogliaro, 644 M. Bearpark, J.J. Heyd, E. Brothers, K.N. Kudin, V.N. Staroverov, R. Kobayashi, J. 645 Normand, K. Raghavachari, A. Rendell, J.C. Burant, S.S. Iyengar, J. Tomasi, M. 646 Cossi, N. Rega, J.M. Millam, M. Klene, J.E. Knox, J.B. Cross, V. Bakken, C. Adamo, 647 J. Jaramillo, R. Gomperts, R.E. Stratmann, O. Yazyev, A.J. Austin, R. Cammi, C. 648 Pomelli, J.W. Ochterski, R.L. Martin, K. Morokuma, V.G. Zakrzewski, G.A. Voth, 649 P. Salvador, J.J. Dannenberg, S. Dapprich, A.D. Daniels, O. Farkas, J.B. Foresman, 650 J.V. Ortiz, J. Cioslowski, and D.J. Fox, Gaussian 09, Revision B.01, Gaussian Inc, 651 Wallingford, CT, 2009.
[23] A.H. Kianfar, S. Asl Khademi, R. Hashemi Fath, M. Roushani, M. Shamsipur, J. Iran. Chem. Soc. 10 (2013) 347–355.
[24] B.S. Garg, D.N. Kumar, Spectrochim. Acta Part A Mol. Biomol. Spectrosc. 59 (2003) 229–234.
[25] A. Anthonysamy, S. Balasubramanian, Inorg. Chem. Commun. 8 (2005) 908–911.
[26] A.H. Kianfar, M. Bahramian, H.R. Khavasi, Spectrochim. Acta Part A 94 (2012) 302–307.
[27] A.H. Kianfar, M. Ebrahimi, Spectrochim. Acta Part A Mol. Biomol. Spectrosc. 115 (2013) 725–729.